Inhibitory effect of nano-targeted micelle administration combined with *in Vitro* radiotherapy on glioma based on nuclear magnetic resonance technology

Ronghui Jin[1], Yingping Xu[2], Pan Jiang[3*]

[1] Department of Radiation, Shaanxi Provincial People's Hospital, Xi'an 710068, Shaanxi Province, China
[2] Radiation Hospital, Shaanxi Cancer Hospital, Xi'an 710061, Shaanxi Province, China
[3] Department of Radiotherapy Area, Shaanxi Cancer Hospital, Xi'an 710061, Shaanxi Province, China

ARTICLE INFO

ABSTRACT

Glioma is a malignant tumor originating from the central nervous system. Glioma is the incidence rate of the central nervous system in adults. Nanotechnology has been widely used in drug delivery in vivo, achieving targeted drug delivery through surface modification. At the same time, the samples measured by NMR have no bias to all compounds, and there is no need for specific internal standards for quantification. Therefore, based on the use of nuclear magnetic resonance technology, this paper analyzed the inhibitory effect of nano-targeted micelles combined with in vitro radiotherapy on glioma. The results show that the coupling constants of β - CH3 of Ala and β - CH3 of Lac are close. It is difficult to distinguish the spectral lines of Ala and Lae by 1.5T NMR. DHA-PLys(s-s)P can efficiently deliver drugs across BBB and into brain parenchymal cells to release drugs. Due to its increased stability in the systemic circulation, DHA-PLys(s-s)P can help to improve drug delivery efficiency. The DNA damage of U87 and U251 cells was more serious than that of C6 cells. There was a positive correlation between DNA damage and Cho/Cr ratio, indicating that nano-targeted micelles combined with in vitro radiotherapy have an inhibitory effect on glioma.

Introduction

Glioblastoma is a kind of primary malignant tumor with a high incidence in adults. Its invasive growth and strong invasiveness often lead to difficult surgical treatment, poor prognosis and easy recurrence. In order to prolong the survival time of glioma patients and improve their quality of life, a reasonable and effective anti-glioma treatment is essential (1). Except for a few gliomas that can spread in the subarachnoid space, there is no extracranial metastasis. However, due to the invasive growth mode of malignant glioma, which is destructive to the nerve tissue, the operation can not be completely removed, and the patient is still facing the threat of death (1-2). Surulescu proposed a multi-scale model of glioma growth, including the interaction between cells and the underlying tissue network and the proliferation effect. Diffusion tensor imaging (DTI) can provide this information, which opens the way for the specific modeling of glioma invasion. Starting from a multi-scale model including subcellular and single cell dynamics, surulescu performs parabolic scaling to obtain the approximate reaction-diffusion-transport equation of tumor cell population at the macro scale. Numerical simulation was conducted based on DTI data to evaluate the performance of surulescu's modeling method (3-4). Kim found that arsenic trioxide significantly upregulated trail death receptor DR5 in glioma cells. The results of the arsenic trioxide study suggest that arsenic trioxide plus TRAIL combined with glioma cells may be an effective and selective treatment strategy (5-6). The purpose of his study was to investigate the expression of neat1 in human gliomas and its relationship with clinicopathological features and prognosis, and to analyze the relationship between the expression of lncrna neat1 and clinicopathological features and prognosis of gliomas. He's research supports neat1 as a potential prognostic predictor, its high expression in tumor tissues and its relationship with glioma carcinogenesis and progression (7-8). The purpose of Ping's study was to investigate the role of cznf292 in the formation of human glioma tubes and its possible mechanism. Ping's research shows that cznf292 silencing plays an important role in the process of glioma tube formation and has the potential as a therapeutic target and biomarker of glioma (9-10). Chai explored the possibility of plasma mir-199a-3p as a biomarker of glioma. Chai found that the overall survival rate of glioma patients with low mir-199a-3p expression levels was significantly shorter than that of patients with high mir-199a-3p expression levels. Univariate and multivariate analysis showed that mir-199a-3p expression was an independent predictor of poor prognosis, and circulating mir-199a-3p could be used as a new biomarker for diagno-

sis and prognosis of glioma (11-12).

Nuclear magnetic resonance (NMR) is a useful tool for elucidating the chemical structure, molecular dynamics and interaction of compounds from organic molecules to mineral and protein complexes (13). W ü RTZ focuses on the application of Mr metabonomics in large-scale epidemiological quantitative circulation biomarkers. W ü RTZ emphasized the molecular characteristics of risk factors, the application of Mendelian randomization, and the key issues in the design and analysis of epidemiological metabolic profiling. W ü RTZ believes that although the large-scale application of metabolic profiling is still a new field, comprehensive biomarker data seem to contribute to the ability to understand the etiology of various diseases and predict disease risk and may be transformed into multiple clinical environments (14-15). Napoli used nuclear magnetic resonance spectroscopy to study the urine metabolic spectrum of patients with PDAC and to detect changes in metabolic spectrum compared with healthy matched controls. The spectral data were analyzed by multivariate statistical technique. Napoli successfully identified the complex molecular characteristics of PDAC by using the NMR analysis of the urine metabolic spectrum. The results of the descriptive level analysis showed that it was possible to track the evolution of the disease and locate the tumor. Given the high repeatability and noninvasive nature of analytical procedures, Napoli's method has the potential to influence large-scale screening procedures (16-17). Liu studied the carbon skeleton characteristics of ultra-fine pulverized coal by nuclear magnetic resonance (NMR) and c-13nmr and studied the changes of coal chemical properties after demineralization. Liu's research shows that in the process of coal pulverization, the research of molecular structure is helpful to better understand the molecular structure of coal, and the data obtained will promote the development of a typical molecular model of ultra-fine pulverized coal and improve its behavior prediction ability in practical application (18-19). Flote measured fasting blood lipid and body mass index (BMI) of 56 female patients aged 35-75 years who were newly diagnosed as stage I / II invasive breast cancer. Flote was used to determine the contents of serum lipoprotein subfractions and their cholesterol, free cholesterol, phospholipids, apolipoprotein A1 and apolipoprotein A2. Flote's results hypothesized the correlation between different lipoprotein subfractions, PGR expression and Ki 67% in breast tumors (20-21). Through the combination of the permeability test and nuclear magnetic resonance test, Lai analyzed the core samples with the tight fluid flow at the pore scale level. Lai has an important understanding of fluid flow in dense porous media through detailed research on imbibition experiments and nuclear magnetic resonance tests (22-23). Yuan discussed the significance of MRI combined with Ki-67 and vascular endothelial growth factor in the diagnosis and prognosis evaluation of glioma. Yuan's research shows that the three combined detections can not only accurately judge the malignant degree of glioma but also effectively evaluate the prognosis of patients, providing a scientific basis for the selection of treatment schemes (24-25).

Radiation therapy can cause DNA damage, and DNA damage can promote cell apoptosis if there is a linear correlation between the changes of metabolites measured by nuclear magnetic resonance spectroscopy and DNA damage. The results of this study not only further suggest that

as a noninvasive method, hydrogen magnetic resonance spectroscopy can reflect the degree of DNA damage after radiotherapy to a certain extent but also can predict cell apoptosis. To analyze the inhibitory effect of nano-targeted micelles combined with in vitro radiotherapy on glioma by nuclear magnetic resonance (NMR) technology so as to provide the basis for clinical radiotherapy effect monitoring and lay a theoretical foundation for the formulation of a clinical individualized radiotherapy scheme.

Materials and Methods

Experimental materials and cell culture

Glioma cell lines: C6 from rats, U87 and u25l from the human. The three cell lines were purchased from the cell resource center of the Municipal Institute of life sciences and stored in the cell room on the third floor of a laboratory in our city. C6 originated from rats and belonged to low-grade gliomas; U87 and U251 originated from human and belonged to high-grade glioma.

The cells were cultured in the culture bottle. The growth of the cells was observed regularly. When the medium turned yellow, the medium changed in time. When the cells grew to about 80% density, the cells were passaged. The cells were subcultured in the biosafety cabinet. The medium was sucked out by the pasteurized pipette and discarded. The cells were washed twice with sterile room temperature PBS. Then, about LML 0.25% trypsin was added into each small culture bottle. After standing, the cells were digested. After a few minutes, the cells were separated from the bottom of the culture bottle and suspended in the culture medium. The cell suspension was aspirated for centrifugation, and then the cells were precipitated. The medium was added, and the pasteurized pipette was fully blown to form a single cell suspension, which was put into a new culture bottle for culture. According to the cell growth rate and cell concentration, the single cell suspension was divided into two or four vials for later use.

Detection of apoptosis rate by flow cytometry and statistical analysis

24h after cell irradiation, when the density grows to about 80%, collect the cells, trypsin digestion and centrifuge to take the cell pellet, wash the cells twice with frozen PBS; resuspend the cells with binding buffer, adjust the concentration to 1.0×10^6/ml, and then draw 100ul Cell suspension into a 5ml test tube; add 5ul FITC-Annexin and 5ul PI, incubate at room temperature, protected from light for 15min, then place the sample in a 4"C refrigerator and wrap it with aluminum foil to achieve the effect of protection from light. Suspend the cells to enhance the staining effect; add 400ul binding buffer, and test the apoptosis rate within 1 hour. Use SPSSl7.0, SigmaPlotl2.0 and other statistical software to analyze the experimental results. The experimental results are indicated by $(x \pm s)$. One-way analysis of variance was used for data comparison among multiple groups, t-test was used for comparison between two sample means, and P<0.05 was considered statistically significant.

Results and Discussion

Analysis of the ratio between the concentrations of metabolites in gliomas

The ratio of Cre / H2O and NAA / CRE was different between high-grade and low-grade gliomas. The metabolite ratio analysis in glioma is shown in Figure 1.

Similar to Lac, when TE was extended from 35 ms to 145 MS, the spectral lines of Ala also reversed. The methyl dipolar signal of Ala cannot be detected in a healthy human brain. It is easy to detect in some brain tumors with elevated Ala. Due to the close coupling constants of β - CH3 of Ala and β - CH3 of Lac, it is difficult to distinguish the spectral lines of Ala and Lae by 1.5T NMR.

Differential diagnosis of intracranial meningiomas based on magnetic resonance spectroscopy has been reported (26).

Quantitative analysis

Flow cytometry was used to determine the cellular uptake efficiency of green BODIPY labeled polymer micelles. The quantitative results were consistent with the qualitative results mentioned above. The uptake of DHA-PLys(s-s)P polymer micelles was 6 times higher than that of unmodified PLys(s-s)P polymer micelles; the uptake of DHA-PLys(s-s)P was decreased by 3 times after adding 10 MMOD glucose, and the uptake of DHA-PLys(s-s)P was inhibited by endocytosis inhibitors, of which the uptake of DHA-PLys(s-s)P was nearly 3 times lower than that of unmodified PLys(s-s)P polymer micelles. The quantitative results of flow cytometry analysis are shown in Figure 2.

PLys(s-s)P has a small amount of signal in the brain, which is similar to that of cells, suggesting that PLys(s-s)P maintains the nature of polymer micelles internalizing into cells. Moreover, due to the small size of polymer micelles, PLys(s-s)P has a greater advantage in crossing BBB. In addition, the accumulation of DHA-PLys(s-s)P was significantly higher than that of PLys(s-s)P after DHA modification, which indicated that the ability of polymer micelles to cross BBB was significantly enhanced by the specific binding of DHA to GLUT l on BBB. The results of brain tissue sections showed that PLys(s-s)P polymer micelles were further absorbed by brain parenchymal cells after crossing BBB and were continuously concentrated in brain parenchymal region. In addition, DHA-PLys(s-s)P can efficiently deliver drugs across BBB and into brain parenchymal cells to release drugs. Because of its stability in vivo circulation, it can help to improve drug delivery efficiency.

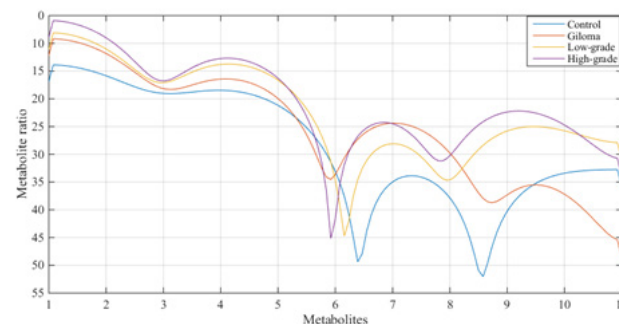Furthermore, Cui et al. (2013) investigated the cellular

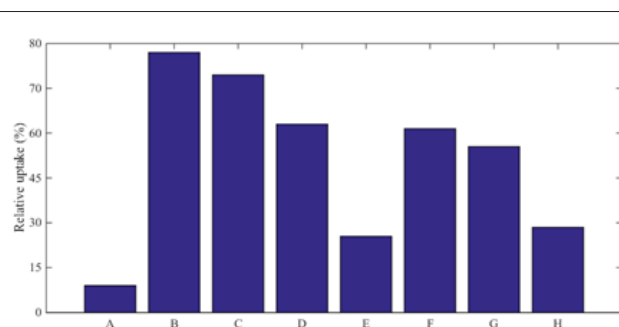**Figure 1.** Analysis of metabolite ratio in glioma.

Figure 2. The quantitative results analyzed by flow cytometric analysis.

uptake, intracellular trafficking and anti-tumor efficacy of doxorubicin-loaded reduction-sensitive micelles (26).

Analysis of nuclear magnetic resonance spectrum and DNA damage characteristics of glioma cell lines

Three kinds of glioma cell lines were irradiated with different doses of X-ray to obtain nuclear magnetic resonance spectroscopy. The statistical results of DNA damage in three cell lines are shown in Table 1.

The nucleus was round, and the tail shape was behind the nucleus. The statistical analysis of DNA damage in three cell lines is shown in Figure 3.

Compared with the control group, as the irradiation dose increased, the DNA damage in the cell line gradually increased; compared with 1Gy, when the irradiation dose was 5Gy, the tail length and tail moment showed significantly different. Compared with 5Gy, the irradiation dose was At 10Gy, and the tail length and tail moment are obviously different; compared with 10Gy when the dose is 15Gy, the difference between C6 and U87 is not statistically significant. Under the same irradiation dose,

Table 1. Statistical results of DNA damage in three cell lines.

Cell line	DNA damage	0Gy	1Gy	5Gy	10Gy	15Gy
C6	Tail length	4.716±3.245	14.145±4.806	17.573±4.523	24.176±3.641	23.753±3.655
	TDNA	10.643±9.834	22.004±11.627	26.971±12.022	34.447±9935	39.716±11.226
	Onunori	0.753±1.094	3.554±2.775	5.174±3.365	8.536±3.144	9.695±3.887
U87	Tail length	0.335±0.546	5.093±3.104	8.965±4.382	17.623±6.465	16.957±6.049
	TDNA	2.563±4.703	17.557±12.143	3.045±3.015	8.625±6.374	8.926±6.64
	Onunori	20.043±6.205	28.843±5.987	33.843±6.983	37.603±7.673	39.922±6.667
U251	Tail length	28.984±6.534	38.077±8.032	45.917±6.917	53.077±9.603	57.702±8.965
	TDNA	28.984±6.538	38.077±8.032	45.917±6.915	53.078±9.602	57.702±8.965
	Onunori	10.736±2.698	17.873±7.357	22.576±6.196	32.985±7.972	42.563±6.903
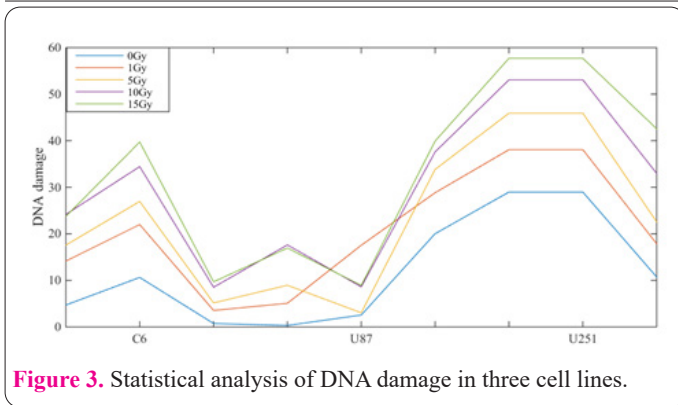
Figure 3. Statistical analysis of DNA damage in three cell lines.

Figure 4. Analysis of dose survival relationship of three glioma cell lines.

the DNA damage of the three cell lines showed significant differences: Compared with C6 and U87, the DNA damage of U25l was heavier, and there were significant differences in tail length, DNA content in the comet tail, and tail moment; In terms of tail length, C6 and U87 showed significant differences; when the irradiation dose was 0Gy, the DNA content in the tails of C6 and U87 was quite different.

Compared with the control group, with the increase of the radiation dose, the DNA damage of the cells gradually increased; compared with 1Gy, the tail length and tail moment at the 5Gy dose were significantly different; compared to 5Gy, the tail length and tail at the 10Gy dose The moment difference is significant. In the long term, there is a significant difference between C6 and U87; when the irradiation dose is 0gy, the DNA damage of U25l is more serious, and the difference in the DNA content of the tail of C6 and U87 is significant.

Li et al. (2017) reported that metabolite changes detected by 1H NMR spectroscopy could be used to determine DNA damage induced by X-ray exposure. 1H NMR spectroscopy is a noninvasive method for predicting DNA damage in glioma cells at the microscopic level (28).

Effect of radiotherapy on normal glial cells and analysis of colony formation

With the increase in X-ray irradiation dose, the apoptosis rate of three glioma cell lines increased gradually. C6 and U87 showed a slow growth trend, while U251 showed a growth trend of first fast and then slow. When the radiation dose was gradually increased, the apoptosis rate and DNA damage showed the same increasing trend. The colony-forming rates of the three glioma cell lines are shown in Table 2.

After the three cell lines were exposed to X-rays of different doses, the colony formation rate was obtained. With the increase of the irradiation dose, the colony formation rate gradually decreased; the colony formation rate was consistent with the trend of apoptosis rate and further promoted cell apoptosis for X-rays. Death provided the basis. The dose survival relationship analysis of the three glioma cell lines is shown in Figure 4.
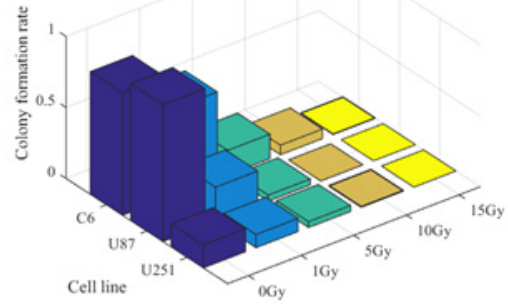
For U87 and u25l, the radiosensitivity of U87 is higher than that of u25l, while the DNA damage is less than u25l, indicating that DNA damage is affected by many other factors besides radiosensitivity. With the increase of radiation dose, lac / Cr and suc / Cr decreased gradually, while Cho / Cr increased gradually, which can reflect the DNA damage at the micro level and further monitor the apoptosis of tumor tissue. The DNA damage of U87 and U251 was more serious than that of C6 cells, and there was a positive correlation between DNA damage and Cho / Cr ratio. Therefore, nano-targeted micelles combined with in vitro radiotherapy have an inhibitory effect on glioma. Measurement of the lactate to creatine ratio by 1 H NMR spectroscopy can be used to non-invasively assess apoptosis in glioma cells following X-ray irradiation (29,30).

In this paper, the change of metabolite ratio of glioma cell line after radiotherapy was measured by nuclear magnetic resonance hydrogen spectrum. The linear correlation between the change of metabolite ratio and DNA damage was preliminarily confirmed. It was also confirmed that nano-targeted micelles combined with in vitro radiotherapy had an inhibitory effect on glioma, which provided microscopic evidence for the clinical application of HMRS as a noninvasive method in the clinical monitoring of the radiotherapy effect.

Our study confirmed the effectiveness of the in vivo proton MRS quantitative detection technique with a non-suppressed water signal as the internal standard. NAA concentration, NAA / H20 ratio and NAA / Cho ratio can be used to distinguish low-grade and high-grade gliomas.

In this paper, there are still some shortcomings, such as the lack of stability in vivo, drug easy to release early, less tumor enrichment, poor tumor cell selectivity and endocytosis efficiency, slow drug release in target cells and other factors that lead to unsatisfactory efficacy. The experiment in this paper is only based on the cell level in vitro, and the effect of in vitro radiotherapy on tumor tissue in vivo is more complex. This paper also needs to combine a large number of animal and clinical experiments so as to provide an important reference for the clinical application of

Table 2. Colony formation rate of three glioma cell lines.

Cell line	0Gy	1Gy	5Gy	10Gy	15Gy
C6	0.863±0.062	0.613±0.042	0.173±0.022	0.0670±0.0030	0.0040±0.0020
U87	0.963±0.053	0.241±0.063	0.043±0.008	0.0003±0.0002	0.0000±0.0000
U251	0.162±0.021	0.093±0.016	0.041±0.002	0.0062±0.0011	0.0003±0.0003

HMRS.

References

1. Zhou Y, Peng Y, Liu M, Jiang Y. MicroRNA-181b Inhibits Cellular Proliferation and Invasion of Glioma Cells via Targeting Sal-Like Protein 4. Oncol Res. 2017 Jul 5;25(6):947-957. doi: 10.3727/096504016X14791732531006. Epub 2016 Nov 17. PMID: 27938503; PMCID: PMC7841051.

2. Jones C, Karajannis MA, Jones DTW, Kieran MW, Monje M, Baker SJ, Becher OJ, Cho YJ, Gupta N, Hawkins C, Hargrave D, Haas-Kogan DA, Jabado N, Li XN, Mueller S, Nicolaides T, Packer RJ, Persson AI, Phillips JJ, Simonds EF, Stafford JM, Tang Y, Pfister SM, Weiss WA. Pediatric high-grade glioma: biologically and clinically in need of new thinking. Neuro Oncol. 2017 Feb 1;19(2):153-161. doi: 10.1093/neuonc/now101. PMID: 27282398; PMCID: PMC5464243.

3. Engwer C, Knappitsch M, Surulescu C. A multiscale model for glioma spread including cell-tissue interactions and proliferation. Math Biosci Eng. 2016 Apr 1;13(2):443-60. doi: 10.3934/mbe.2015011. PMID: 27105989.

4. Buckner JC, Shaw EG, Pugh SL, Chakravarti A, Gilbert MR, Barger GR, Coons S, Ricci P, Bullard D, Brown PD, Stelzer K, Brachman D, Suh JH, Schultz CJ, Bahary JP, Fisher BJ, Kim H, Murtha AD, Bell EH, Won M, Mehta MP, Curran WJ Jr. Radiation plus Procarbazine, CCNU, and Vincristine in Low-Grade Glioma. N Engl J Med. 2016 Apr 7;374(14):1344-55. doi: 10.1056/NEJMoa1500925. PMID: 27050206; PMCID: PMC5170873.

5. Liu SY, Wen CY, Lee YJ, Lee TC. XPC silencing sensitizes glioma cells to arsenic trioxide via increased oxidative damage. Toxicol Sci. 2010 Jul;116(1):183-93. doi: 10.1093/toxsci/kfq113. Epub 2010 Apr 19. PMID: 20403967.

6. Yue X, Lan F, Hu M, Pan Q, Wang Q, Wang J. Downregulation of serum microRNA-205 as a potential diagnostic and prognostic biomarker for human glioma. J Neurosurg. 2016 Jan;124(1):122-8. doi: 10.3171/2015.1.JNS141577. Epub 2015 Jul 31. PMID: 26230475.

7. He C, Jiang B, Ma J, Li Q. Aberrant NEAT1 expression is associated with clinical outcome in high grade glioma patients. APMIS. 2016 Mar;124(3):169-74. doi: 10.1111/apm.12480. Epub 2015 Nov 19. PMID: 26582084.

8. Bush NA, Chang SM, Berger MS. Current and future strategies for treatment of glioma. Neurosurg Rev. 2017 Jan;40(1):1-14. doi: 10.1007/s10143-016-0709-8. Epub 2016 Apr 16. PMID: 27085859.

9. Yang P, Qiu Z, Jiang Y, Dong L, Yang W, Gu C, Li G, Zhu Y. Silencing of cZNF292 circular RNA suppresses human glioma tube formation via the Wnt/β-catenin signaling pathway. Oncotarget. 2016 Sep 27;7(39):63449-63455. doi: 10.18632/oncotarget.11523. PMID: 27613831; PMCID: PMC5325376.

10. Zhang R, Pang B, Xin T, Guo H, Xing Y, Xu S, Feng B, Liu B, Pang Q. Plasma miR-221/222 Family as Novel Descriptive and Prognostic Biomarkers for Glioma. Mol Neurobiol. 2016 Apr;53(3):1452-1460. doi: 10.1007/s12035-014-9079-9. Epub 2015 Jan 31. PMID: 25636684.

11. Chai C, Song LJ, Yang B, Han SY, Li XQ, Li M. Circulating miR-199a-3p in plasma and its potential diagnostic and prognostic value in glioma. Eur Rev Med Pharmacol Sci. 2016 Dec;20(23):4885-4890. PMID: 27981547.

12. Hamard L, Ratel D, Selek L, Berger F, van der Sanden B, Wion D. The brain tissue response to surgical injury and its possible contribution to glioma recurrence. J Neurooncol. 2016 May;128(1):1-8. doi: 10.1007/s11060-016-2096-y. Epub 2016 Mar 9. PMID: 26961772.

13. Horton D, Lauterbach JH. Correction to "Relative Reactivities of Hydroxyl Groups in Carbohydrate Derivatives. Specific Nuclear Magnetic Resonance Spectral Assignments of Acetyl Groups in Methyl α-d-Glucopyranoside Tetraacetate and Related Derivatives". J Org Chem. 2018 Feb 2;83(3):1686. doi: 10.1021/acs.joc.8b00018. Epub 2018 Jan 23. PMID: 29359555.

14. Würtz P, Kangas AJ, Soininen P, Lawlor DA, Davey Smith G, Ala-Korpela M. Quantitative Serum Nuclear Magnetic Resonance Metabolomics in Large-Scale Epidemiology: A Primer on -Omic Technologies. Am J Epidemiol. 2017 Nov 1;186(9):1084-1096. doi: 10.1093/aje/kwx016. PMID: 29106475; PMCID: PMC5860146.

15. Kycia JB, Haard TM, Rand MR, Hensley HH, Moores GF, Lee Y, Hamot PJ, Sprague DT, Halperin WP, Thuneberg EV. High-resolution nuclear magnetic resonance of superfluid 3He-B. Phys Rev Lett. 1994 Feb 7;72(6):864-867. doi: 10.1103/PhysRevLett.72.864. PMID: 10056554.

16. Napoli C, Sperandio N, Lawlor RT, Scarpa A, Molinari H, Assfalg M. Urine metabolic signature of pancreatic ductal adenocarcinoma by (1)h nuclear magnetic resonance: identification, mapping, and evolution. J Proteome Res. 2012 Feb 3;11(2):1274-83. doi: 10.1021/pr200960u. Epub 2011 Nov 28. PMID: 22066465.

17. Nishimura K, Ohya S, Mutsuro N. Nuclear magnetic resonance on oriented 99m, 101m, 102 Rh and 101 Pd. Nuclear Physics A. 1986 Mar 24;451(2):233-42.

18. Liu J, Jiang X, Shen J, Zhang H. Chemical properties of superfine pulverized coal particles. Part 1. Electron paramagnetic resonance analysis of free radical characteristics. Adv Powder Technol 2014;25(3):916-25.

19. Wang Q, Jin J, Dai N, Han N, Han J, Bao B. Anti-inflammatory effects, nuclear magnetic resonance identification, and high-performance liquid chromatography isolation of the total flavonoids from Artemisia frigida. J Food Drug Anal. 2016 Apr;24(2):385-391. doi: 10.1016/j.jfda.2015.11.004. Epub 2016 Jan 6. PMID: 28911593; PMCID: PMC9339558.

20. Flote VG, Vettukattil R, Bathen TF, Egeland T, McTiernan A, Frydenberg H, Husøy A, Finstad SE, Lømo J, Garred Ø, Schlichting E, Wist EA, Thune I. Lipoprotein subfractions by nuclear magnetic resonance are associated with tumor characteristics in breast cancer. Lipids Health Dis. 2016 Mar 12;15:56. doi: 10.1186/s12944-016-0225-4. PMID: 26970778; PMCID: PMC4789271.

21. Schoeters E, Geenen J, Nuytten C, Vanneste L, Cogneau M. Nuclear polarization and nuclear magnetic resonance of 123I and 125I. Nuclear Physics A. 1979 Jul 2;323(1):1-2.

22. Lai F, Li Z, Wei Q, Zhang T, Zhao Q. Experimental investigation of spontaneous imbibition in a tight reservoir with nuclear magnetic resonance testing. Energy Fuels 2016 Nov 17;30(11):8932-40.

23. Steinmann C, Bratholm LA, Olsen JM, Kongsted J. Automated Fragmentation Polarizable Embedding Density Functional Theory (PE-DFT) Calculations of Nuclear Magnetic Resonance (NMR) Shielding Constants of Proteins with Application to Chemical Shift Predictions. J Chem Theory Comput. 2017 Feb 14;13(2):525-536. doi: 10.1021/acs.jctc.6b00965. Epub 2017 Jan 3. PMID: 27992211.

24. Yuan X, Liu D, Wang Y, Li X. Significance of nuclear magnetic resonance combined with Ki-67 and VEGF detection in the diagnosis and prognosis evaluation of brain glioma. J BUON. 2018 Mar-Apr;23(2):410-415. PMID: 29745085.

25. Rennella E, Sekhar A, Kay LE. Self-Assembly of Human Profilin-1 Detected by Carr-Purcell-Meiboom-Gill Nuclear Magnetic Resonance (CPMG NMR) Spectroscopy. Biochemistry. 2017 Feb 7;56(5):692-703. doi: 10.1021/acs.biochem.6b01263. Epub 2017 Jan 20. PMID: 28052669.

26. Jaskólski DJ, Fortuniak J, Stefańczyk L, Majos A, Gajewicz W,

Papierz W, Liberski PP, Sikorska B. Differential diagnosis of intracranial meningiomas based on magnetic resonance spectroscopy. Neurol Neurochir Pol. 2013 May-Jun;47(3):247-55. doi: 10.5114/ninp.2013.32998. PMID: 23821422.

27. Cui C, Xue YN, Wu M, Zhang Y, Yu P, Liu L, Zhuo RX, Huang SW. Cellular uptake, intracellular trafficking, and antitumor efficacy of doxorubicin-loaded reduction-sensitive micelles. Biomaterials. 2013 May;34(15):3858-69. doi: 10.1016/j.biomaterials.2013.01.101. Epub 2013 Feb 26. PMID: 23452389.

28. Li H, Xu Y, Shi W, Li F, Zeng Q, Yi C. Assessment of alterations in X-ray irradiation-induced DNA damage of glioma cells by using proton nuclear magnetic resonance spectroscopy. Int J Biochem Cell Biol. 2017 Mar;84:109-118. doi: 10.1016/j.biocel.2017.01.010. Epub 2017 Jan 22. PMID: 28122253.

29. Dhuldhaj UP, Malik N. Global perspective of phosphate solubilizing microbes and phosphatase for improvement of soil, food and human health. Cell Mol Biomed Rep 2022 Sep 1;2(3):173-86.

30. Li H, Cui Y, Li F, Shi W, Gao W, Wang X, Zeng Q. Measuring the lactate-to-creatine ratio via 1H NMR spectroscopy can be used to noninvasively evaluate apoptosis in glioma cells after X-ray irradiation. Cell Mol Biol Lett. 2018 Jun 15;23:27. doi: 10.1186/s11658-018-0092-2. PMID: 29946338; PMCID: PMC6003206.